Carbon Nanotubes Supported Mesoporous Mesocrystals of Anatase TiO_2

Bin Liu and Hua Chun Zeng*

Department of Chemical and Biomolecular Engineering and Minerals, Metals, and Materials Technology Center, Faculty of Engineering, National University of Singapore, 10 Kent Ridge Crescent, Singapore 119260

Received January 6, 2008. Revised Manuscript Received January 22, 2008

Carbon nanotubes (CNTs) and titanium dioxides (TiO_2) are among the most studied functional materials in recent years. In this work, we have developed a one-pot chemical approach to prepare mesocrystals of anatase TiO_2 onto multiwalled CNTs with controllable surface coverage, surface area, crystal orientation, and TiO_2/CNTs ratio. Under mild reaction conditions (at 60 °C and slightly higher than 1 atm), [001]-oriented petal-like TiO_2 mesocrystals have been evenly grown onto CNTs in aqueous solution. The overlayer metal-oxide phase has crystallite sizes of 2−4 nm and a very uniform size of mesopores centered at 2.5 nm. Some possible mechanisms for pore formation under this surfactant-free condition are discussed. Our investigation also indicates that the CNTs supported mesocrystals of anatase TiO_2 can be used as composite catalysts, and they have been proved to be highly active and robust for photocatalytic degradation of methyl orange, without any additional treatments.

Introduction

Carbon nanotubes (CNTs) and nanostructured titanium dioxide (TiO_2) are among the most investigated functional materials over the past 15 years or so,[1–11] because of their many outstanding physicochemical properties in electrical, optical, mechanical, catalytic, and sensing applications. In recent years, efforts have also been devoted to fabricating these two materials into TiO_2/CNTs nanocomposites, aiming at a synergetic combination of their intrinsic properties and thus enhanced performance to meet new requirements imposed by advanced applications such as optoelectronic quantum dot arrays, solar energy utilization, and heterogeneous photocatalysis etc.[12–29] Generally speaking, in most of these nanocomposites, CNTs serve as a core support for TiO_2 while the latter is often prepared as an overlayer, resembling cable-like sheathed structures (i.e., CNTs supported TiO_2). Among the many reported methods for this binary composite, sol–gel coating, followed by a heat-treatment at elevated temperatures, is the most commonly adopted method to introduce the inorganic phase onto the CNTs substrate,[12–19] compared to other techniques such as chemical and physical vapor depositions,[20,21] hydrothermal and solvothermal syntheses,[22–24] sonochemical processing,[25] electrospinning,[26] self-assembly, and so forth.[27–29]

Despite the significant advancement, many technical issues related to the above process methods remain to be addressed.[12–29]

* Corresponding author. Tel.: (65) 6516-2896. Fax: (65) 6779-1936. E-mail: chezhc@nus.edu.sg.

(1) Iijima, S. *Nature* **1991**, *354*, 56–58.
(2) Ebbesen, T. W.; Ajayan, P. M. *Nature* **1992**, *358*, 220–222.
(3) Ajayan, P. M.; Ebbesen, T. W. *Rep. Prog. Phys.* **1997**, *60*, 1025–1062.
(4) Subramoney, S. *Adv. Mater.* **1998**, *10*, 1157–1171.
(5) Thess, A.; Lee, R.; Nikolaev, P.; Dai, H.; Petit, P.; Robert, J.; Xu, C.; Lee, Y. H.; Kim, S. G.; Rinzler, A. G.; Colbert, D. T.; Scuseria, G. E.; Tománek, D.; Fischer, J. E.; Smalley, R. E. *Science* **1996**, *273*, 483–487.
(6) Kamat, P. V. *J. Phys. Chem. C* **2007**, *111*, 2834–2860.
(7) (a) Penn, R. L.; Banfield, J. F. *Science* **1998**, *281*, 969–971. (b) Cozzoli, P. D.; Kornowski, A.; Weller, H. *J. Am. Chem. Soc.* **2003**, *125*, 14539–14548.
(8) Jun, Y.-W.; Casula, M. F.; Sim, J.-H.; Kim, S. Y.; Cheon, J.; Alivisatos, A. P. *J. Am. Chem. Soc.* **2003**, *125*, 15981–15985.
(9) Zhou, Y.; Antonietti, M. *J. Am. Chem. Soc.* **2003**, *125*, 14960–14961.
(10) Yang, H. G.; Zeng, H. C. *Angew. Chem., Int. Ed.* **2004**, *43*, 5206–5209.
(11) Kröger, N.; Dickerson, M. B.; Ahmad, G.; Cai, Y.; Haluska, M. S.; Sandhage, K. H.; Poulsen, N.; Sheppaard, V. C. *Angew. Chem., Int. Ed.* **2006**, *45*, 7239–7243.
(12) Moriguchi, I.; Hidaka, R.; Yamada, H.; Kudo, T.; Murakami, H.; Nakashima, N. *Adv. Mater.* **2006**, *18*, 69–73.
(13) Yang, Y. D.; Qu, L. T.; Dai, L. M.; Kang, T.-S.; Durstock, M. *Adv. Mater.* **2007**, *19*, 1239–1243.
(14) Guirado-López, R. A.; Sánchez, M.; Rincón, M. E. *J. Phys. Chem. C* **2007**, *111*, 57–65.
(15) Yan, X. B.; Tay, B. K.; Yang, Y. *J. Phys. Chem. B* **2006**, *110*, 25844–25849.
(16) Lu, X.; Imae, T. *J. Phys. Chem. C* **2007**, *111*, 8459–8462.
(17) Yu, H. T.; Quan, X.; Chen, S.; Zhao, H. M. *J. Phys. Chem. C* **2007**, *111*, 12987–12991.
(18) Wang, W. D.; Serp, P.; Kalck, P.; Faria, J. L. *J. Mol. Catal. A: Chem.* **2005**, *235*, 194–199.
(19) Jitianu, A.; Cacciaguerra, T.; Benoit, R.; Delpeux, S.; Béguin, F.; Bonnamy, S. *Carbon* **2004**, *42*, 1147–1151.
(20) Orlanducci, S.; Sessa, V.; Terranova, M. L.; Battiston, G. A.; Battiston, S.; Gerbasi, R. *Carbon* **2006**, *44*, 2839–2843.
(21) Fan, W. G.; Gao, L.; Sun, J. *J. Am. Ceram. Soc.* **2006**, *89*, 731–733.
(22) Lee, S.-W.; Sigmund, W. M. *Chem. Commun.* **2003**, 780–781.
(23) Wang, Z. Y.; Ergang, N. S.; Al-Daous, M. A.; Stein, A. *Chem. Mater.* **2005**, *17*, 6805–6813.
(24) An, G. M.; Ma, W. H.; Sun, Z. Y.; Liu, Z. M.; Han, B. X.; Miao, S. D.; Miao, Z. J.; Ding, K. L. *Carbon* **2007**, *45*, 1795–1801.
(25) Yu, Y.; Yu, J. C.; Yu, J.-G.; Kwok, Y.-C.; Che, Y.-K.; Zhao, J.-C.; Ding, L.; Ge, W.-K.; Wong, P.-K. *Appl. Catal., A* **2005**, *289*, 186–196.
(26) Kedem, S.; Schmidt, J.; Paz, Y.; Cohen, Y. *Langmuir* **2005**, *21*, 5600–5604.
(27) Li, H. X.; Niu, J. L.; Zhang, J.; Li, H. L.; Liu, Z. F. *J. Phys. Chem. B* **2003**, *107*, 2453–2458.
(28) Shin, H. S.; Jang, Y. S.; Lee, Y.; Jung, Y.; Kim, S. B.; Choi, H. C. *Adv. Mater.* **2007**, *19*, 2873–2876.
(29) Li, J.; Tang, S. B.; Lu, L.; Zeng, H. C. *J. Am. Chem. Soc.* **2007**, *129*, 9401–9409.

10.1021/cm800040k CCC: $40.75
Published on Web 03/18/2008

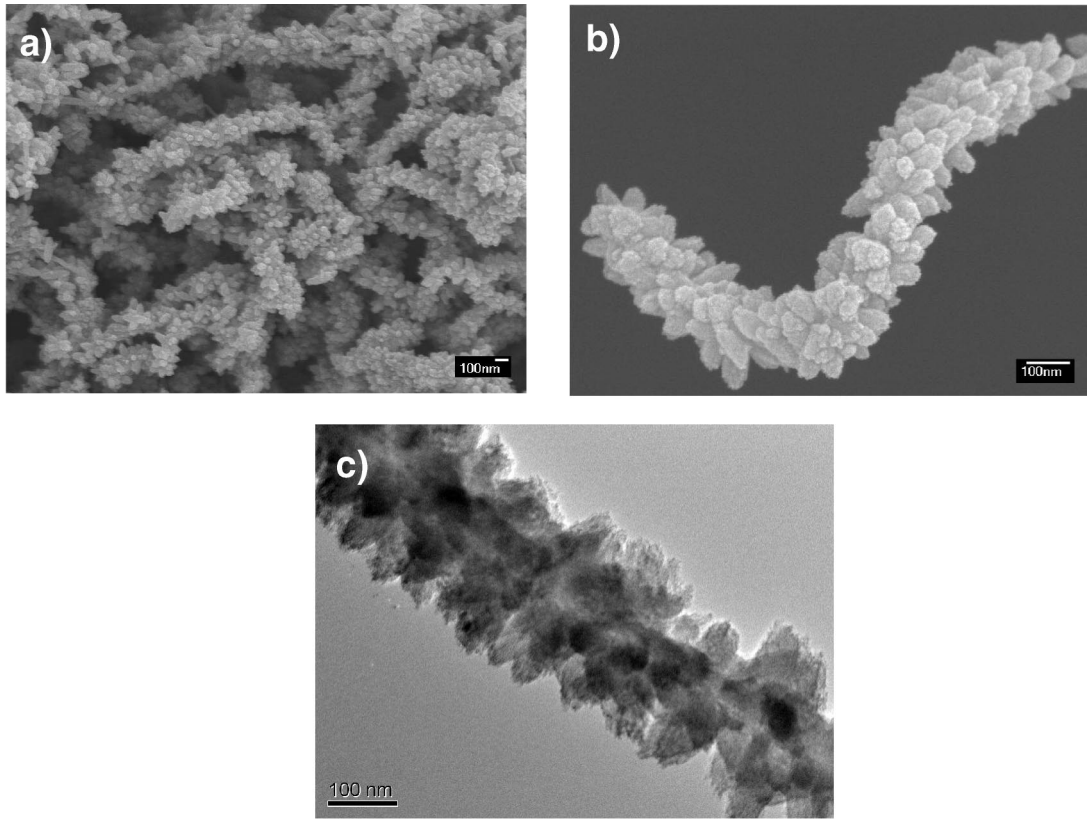

Figure 1. Mesoporous TiO_2/CNTs nanocomposites prepared in this work (Sample A): (a) panoramic views at low magnification (FESEM image), (b) a single strand of TiO_2/CNTs at higher magnification (FESEM image), and (b) TEM image of a TiO_2/CNTs strand in which central space of CNT support is visible.

For instance, the heat-treatment required in sol–gel processes often causes the phase detachment between surface TiO_2 and underneath CNTs. Furthermore, agglomeration among neighboring TiO_2/CNTs cables and nonuniform crystallite and pore sizes of the overlayer are the two major technical drawbacks associated to the techniques that require high-temperature treatments. Although the self-assembly is a promising soft approach, on the other hand, its process difficulties at the present time are overcoat discontinuity and lack of orientation control over the oxide crystallites. In this work, we develop a facile liquid phase deposition method that can be operated under mild reaction conditions (at 60 °C and slightly higher than 1 atm). For the first time, mesocrystalline anatase TiO_2 has been grown directly onto the CNTs support, with their protruding petal-like morphology along the [001] crystallographic orientation. Furthermore, high specific surface area, uniform crystallite size, and narrow single-modal pore-size distribution have been achieved with this wet chemical process. Our preliminary investigation also indicates that the prepared TiO_2/CNTs are sufficiently active and robust for photocatalytic degradation of organic compounds.

Experimental Section

Materials Preparation. In a typical synthesis reported in this work, 15 mg of multiwalled carbon nanotubes (CNTs; from Aldrich, without further treatment) was added to 20 mL of 0.04 M of TiF_4 solution (pH = 1.69) in a glass beaker (100 mL). The glass beaker was then sealed with parafilm and held over an ultrasonic water bath for 30 min. Afterward the mixture was kept inside an electric oven at 60 °C for 20 h. After reaction, the parafilm was found broken, due to the build-up pressure upon the reaction. The products were washed three times with deionized water and one time with pure ethanol, and collected by normal sedimentation, followed by vacuum-drying. The thus obtained sample is named Sample A. To understand the effect of pressure, similar experiments were also carried out using a glass culture bottle (100 mL; screwed with a pressure-tight plastic cap) and an open glass beaker (100 mL; without parafilm sealing), respectively. In the synthesis in a closed reactor, 15 mg of CNTs was added to 20 mL of 0.04 M TiF_4 solution at pH = 1.69 in a glass culture bottle. The mixture was sealed with the plastic cover and held over an ultrasonic water bath for 1 min. Afterward the mixture was placed inside an electric over at 60 °C for 24 h. The culture bottle was kept sealed during reaction. After the reaction, the culture bottle was still kept sealed properly. The sample prepared underwent the same treatments of washing and drying, and is denoted as Sample B in this work. In the synthesis in an open system, 15 mg of CNTs was added to 20 mL of 0.04 M TiF_4 solution at pH = 1.69 in a normal glass beaker. The mixture was sealed with parafilm and held over an ultrasonic water bath for 60 min, and soon after this, the mixture was kept inside an electric over at 60 °C for 4 h, noting that the beaker was left open during the 4 h of reaction.

Photodegradation Reactions. In a typical experiment, 20 mg of a studied TiO_2/CNTs composite catalyst, or pure CNTs (as a reference experiment), was added to 45.0 mL of deionized water in a 125 mL conical flask. The mixture was ultrasonicated over a water bath for 30 min to ensure a good dispersion of the catalysts, followed by adding 5.0 mL of a methyl orange solution ($C_{14}H_{14}N_3NaO_3S$; 100 mg/L) which had been bubbled with purified air for 1 h prior to use. The mixture was sealed and stirred at room

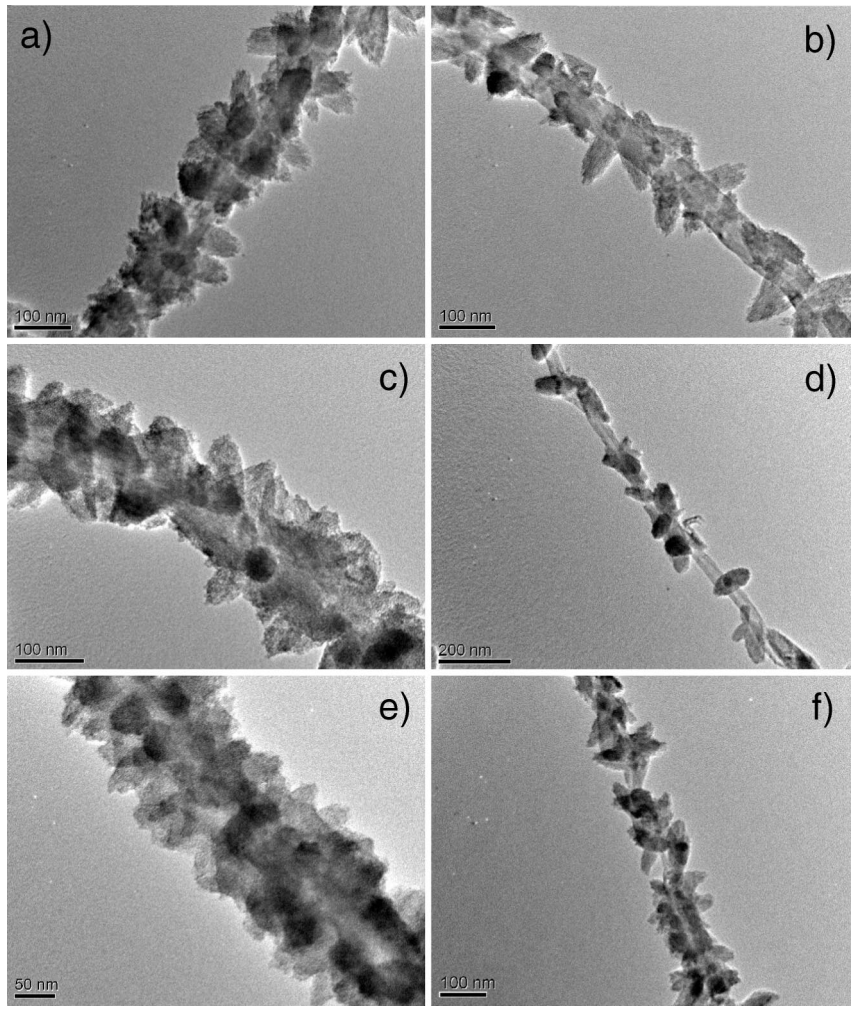

Figure 2. TiO_2/CNTs product morphologies (TEM images) from three series of experiments conducted with different sonication times (a, b, 1 min; c, d, 30 min; e, f, 60 min) and a shorter growth time of 4 h. Other experimental parameters were kept identical to those used for Sample A.

temperature for 2 h in order to achieve adsorption equilibrium for methyl orange. The mixture was later illuminated with a Hg lamp (125 W; Philips) with a cutoff filter ($\lambda = 360$ nm) for 60 min, during which a volume of 2.0 mL of solution together with the catalyst was drawn out every 10 min to determine the concentration of remaining reactant using UV–visible spectrophotometry; the solution was separated from the catalyst by centrifugation. For comparison purposes, commercial TiO_2 powders (P25; from Degussa) was also tested as a reference. Because adsorption of methyl orange on P25 was not severe, the methyl orange solution (100 mg/L) used in the reaction was reduced to 3.2 mL (while deionized water to 46.8 mL) in order to attain a similar initial concentration for all tests. Chemical stability of the TiO_2/CNTs catalyst was further tested after one cycle of the reaction. In this test, the used catalyst after separation was mixed immediately with a newly prepared methyl orange solution [46.9 mL of deionized water and 3.1 mL of the methyl orange solution (100 mg/L); methyl orange herein was further decreased to 3.1 mL because the used catalyst had adsorbed some methyl orange molecules from the previous run]. Then the photocatalysis reaction was repeated under the same condition.

Materials Characterization. The morphological, structural, and compositional information of the studied TiO_2/CNTs samples were obtained with field-emission scanning electron microscopy, energy-dispersive X-ray spectroscopy (FESEM/EDX, JSM-6700F), transmission electron microscopy, selected area electron diffraction, (TEM/SAED/EDX, JEM-2010, 200 kV), and high-resolution transmission electron microscopy (HRTEM, JEM-2010F, 200 kV). Thermal behavior of samples was analyzed using thermogravimetric method (TGA, TA instrument TGA 2050). About 6−8 mg of samples was heated with an air flow of 100 mL/min and at a heating rate of 10 °C/min from room temperature to 900 °C. The nitrogen adsorption/desorption isotherms of the as-prepared samples and pristine CNTs were measured on a Quantachrome NOVA-3000 system at 77 K. Prior to measurements, the samples were degassed at 353 K overnight. X-ray photoelectron spectroscopy (XPS, AXIS-HSi, Kratos Analytical) was used to investigate surface composition of the as-prepared TiO_2/CNTs samples. The spectra of all interested elements were referenced to the C 1s peak arising from adventitious carbon (its binding energy was set at 284.6 eV). As mentioned above, the concentration of methyl orange during photodegradation reaction was monitored with a UV–vis−near-IR scanning spectrophotometer (Shimadzu UV-3101PC).

Results and Discussion

Figure 1 shows a typical mesoporous TiO_2/CNTs sample synthesized under optimized conditions. As can be seen, pristine CNTs are covered with closely arranged petal-like TiO_2 crystallites (Figure 1a). Apparently, adjacent strands do not grow into each other, showing a discrete product morphology (Figure 1b,c). The average diameter of this cable-like composite structure is in the range of 150–200 nm depending on the original diameter of CNTs, and its

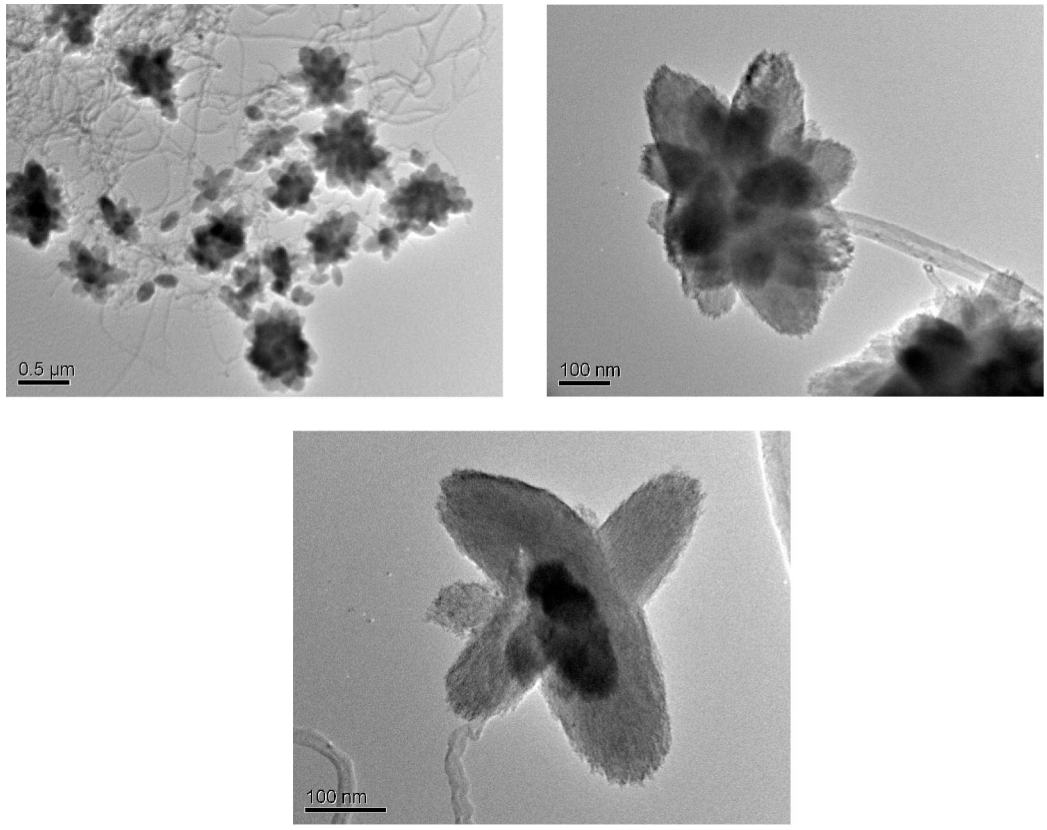

Figure 3. Flowerlike TiO_2 grown on CNTs (Sample B) in tightly capped glass culture bottle (TEM images). See Experimental Section for growth conditions.

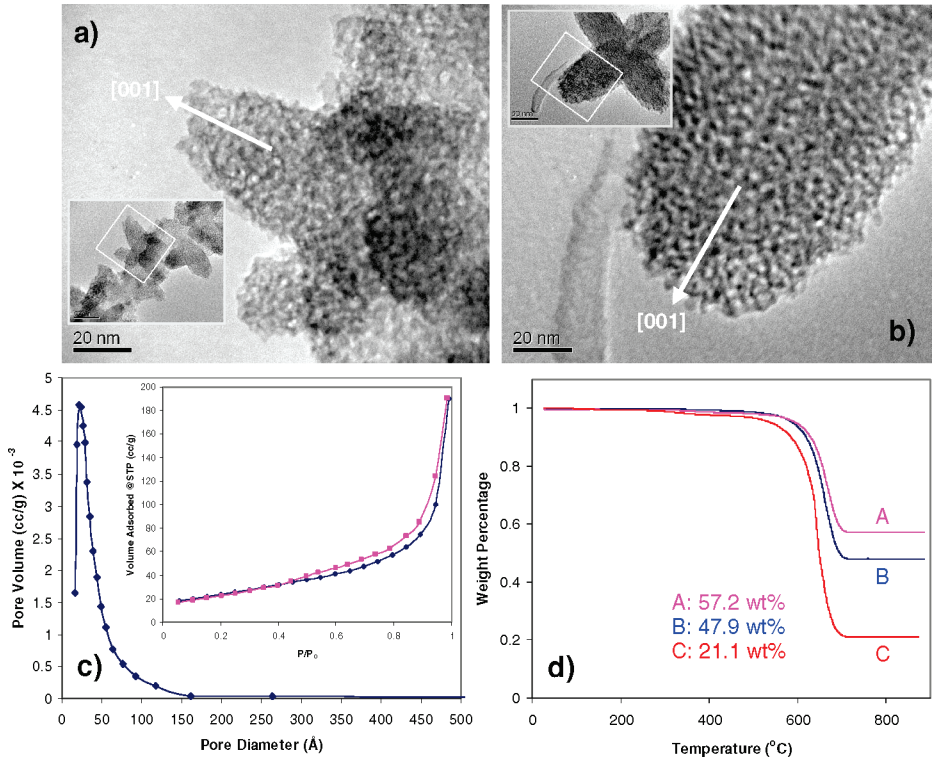

Figure 4. Characterization of mesoporous TiO_2/CNTs nanocomposites: (a, b) mesoporous structure of TiO_2 petal (TEM images; the examined location is indicated with a dotted frame in the inset images; a, 4 h of growth; and b, 24 h of growth), (c) isothermal nitrogen adsorption–desorption loop and BJH pore size distribution (Sample A), and (d) TGA scans of three TiO_2/CNTs samples: A (Sample A), B (Sample B), and C (similar to Sample A, but with a shorter reaction time of 4 h); refer to Experimental Section for details.

hollow nature (i.e., central CNTs, Supporting Information, SI-1) can be further affirmed with transmission electron microscopy (TEM, Figure 1c). Detailed examinations on the interface regions between TiO_2 and CNTs with FSEM and

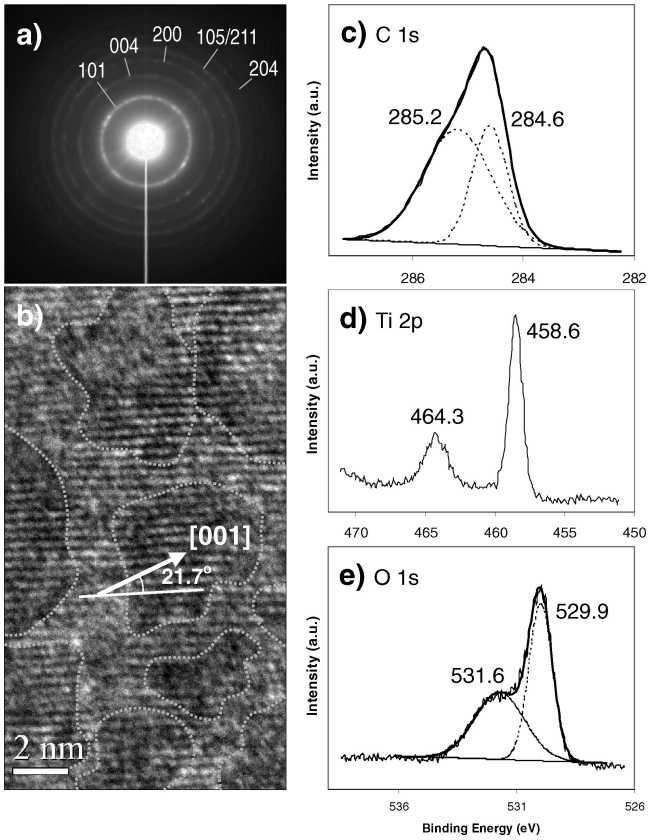

Figure 5. Structural and surface investigation of mesoporous TiO_2/CNTs nanocomposites (Sample A): (a) an electron diffraction pattern for the as-prepared ample; (b) a detailed view (HRTEM image, lattice fringes $d_{101} = 3.5 \pm 0.1$ Å) on an anatase TiO_2 petal mesocrystal; and (c−e) XPS spectra of C 1s, Ti 2p, and O 1s. In (b), the dotted grey lines indicate the image contrasts among the crystallites, and the arrow points to the main assembling direction of the petal, which is 21.7° away from the {101} planes.

TEM techniques indicate that the two phases are intimately attached in the composites (SI-2). In order to investigate the effects of process parameters on the nucleation and growth of TiO_2, different sets of experiments were further carried out. For example, it has been well know that more defect sites on the surface of CNTs can be made with sonication treatments. To investigate required surface defects, three series of experiments were conducted by varying sonication time used, while keeping other growth parameters unaltered. As shown in Figure 2, after a shorter reaction time of 4 h, very similar TiO_2/CNTs products with both fully covered and partially covered CNTs were prepared regardless of the length of sonication. Therefore, the sonication time is not important in these syntheses. Because the defect sites of CNTs are well conceived as heterogeneous nucleation sites for a secondary phase, it is understandable that there had been sufficient defect sites in CNTs for the initial TiO_2 nucleation.[27,29] Under the similar conditions, the concentration of TiF_4 precursor in the starting solution does not play a major role either. Nonetheless, the reaction time clearly governs the deposition of TiO_2 on the carbon substrate. In shorter reactions, as have shown in Figure 2, uncovered segments of CNTs can still be found (Figure 2b,d,f). It is further noted that the following hydrolysis reaction is responsible for the formation of TiO_2 phase: [10]

$$TiF_4 + 2H_2O \leftrightarrow TiO_2(s) + 4HF(g) \quad (1)$$

If the gaseous product HF can be released during the growth, the reaction proceeds toward right-hand side, i.e., more TiO_2 could be formed (which was the normal conditions adopted in this work). However, when the reaction is carried out with a closed batch process (Experimental Section; Sample B), much less TiO_2 is obtained because the HF cannot be timely released from the system and the forward reaction became more difficult. Figure 3 displays some representative TEM images of Sample B. It is clearly demonstrated that the TiO_2 mesocrystals were only grown in limited locations of CNTs, while the sizes of these flowerlike structures are about 5 times as large as the diameters of TiO_2-coated CNTs reported in Figure 1.

It is rather surprising to note that the inorganic phase synthesized under our synthetic conditions comprises numerous tiny TiO_2 crystallites in the range of only 2–4 nm even without introducing any surfactants in our synthesis, as revealed in the image contrasts of Figure 4a,b (also see Figure 5b and Supporting Information, SI-4, later). Crystallinity can benefit from a longer process, because of Ostwald ripening (e.g., Figure 4b).[30] The nanocrystallites in the petals seem to be well connected, leaving very uniform intercrystallite pores. To further explore this, we used Brunauer–Emmett–Teller and Barrett–Joyner–Halenda (BET/BJH) methods to determine specific surface area and porosity. In Figure 4c, a nitrogen isotherm (adsorption–desorption loop) on this sample is displayed. The hysteresis loop typically belongs to type H3, indicating the characteristic of mesoporous materials. Our BET measurement indicates that the prepared TiO_2/CNTs composite have a specific surface area of 116 m^2/g (i.e., Sample A), which is much higher than that of the support CNTs alone (41 m^2/g). More interestingly, a single peak in BJH pore distribution at 25 Å is observed, which indicates that very uniform mesopores can be attained with this simple method. Chemical stoichiometry of TiO_2 has also been checked with energy dispersive X-ray spectroscopy (EDX, SI-3). On the other hand, the weight ratio between the TiO_2 and CNTs in the composites can be easily determined by thermogravimetric analysis (TGA), because CNTs can be readily burnt away in air atmosphere at around 663 °C (SI-3), as reported in Figure 4d. Upon the removal of CNTs, the color of samples changed from black gray to white, resulting in phase-pure rutile TiO_2 (also see Figure 6 later). Since interior CNTs were accessible to air molecules in this combustion, it is deduced that the mesopores in the TiO_2 are interconnected. The actual specific surface for the porous TiO_2 could be further estimated when the composition of a nanocomposite is known. For example, the specific surface area for the TiO_2 overlayer in Sample A is larger than 172 m^2/g (of TiO_2), derived from the measured data 116 m^2/g (of 57.2 wt % TiO_2/42.8 wt % CNTs) and 41 m^2/g (of CNTs).

The crystallographic structure of resultant TiO_2/CNTs was characterized by selected area electron diffraction (SAED). Displayed in Figure 5a is a SAED pattern taken from an as-prepared TiO_2/CNTs sample. Though they are not strong

(30) Yang, H. G.; Zeng, H. C. *J. Phys. Chem. B* **2004**, *108*, 3492–3495.

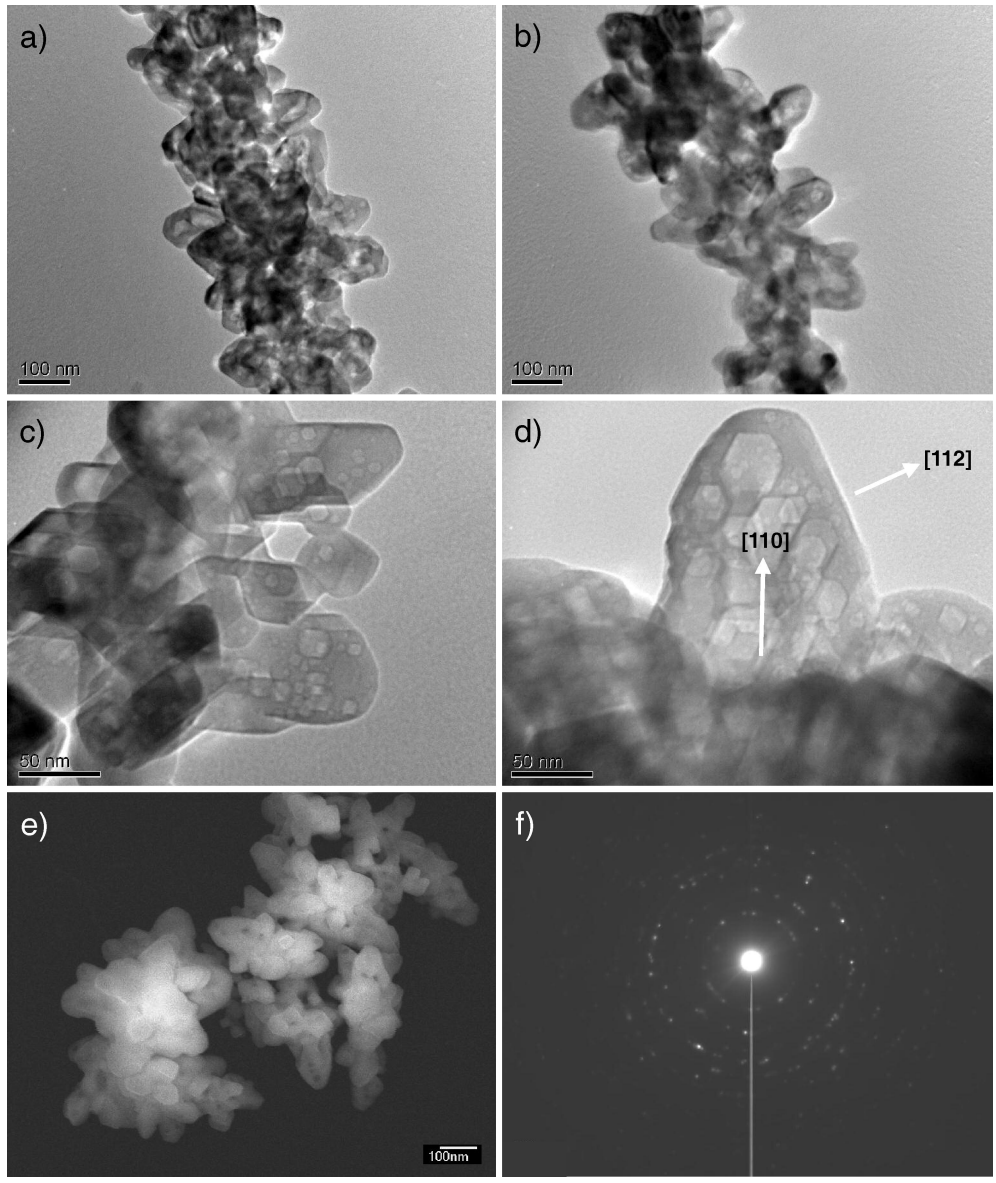

Figure 6. Rutile TiO_2 product obtained from a TiO_2/CNTs nanocomposite precursor (after heating Sample A in a TGA station from room temperature to 900 °C): (a−d) TEM images, (e) SEM image, and (f) SAED rings of rutile phase.

(due to tiny crystallite sizes; except for the 101 ring, which also overlaps with the 0002 diffraction of CNTs), the diffraction rings can be indexed perfectly to the anatase phase of TiO_2 (space group: $I4_1/amd$; tetragonal symmetry, a_o = 3.7852 Å and c_o = 9.5139 Å, JCPDS file no. 21-1272).[29,30] Consistent with the observed mesoporosity (Figure 4a,b), our high-resolution TEM investigation in Figure 5b indicates the crystallites of TiO_2 are indeed in the sizes of 2–4 nm with through pore structures formed by them, as can be verified from the contrasts in the HRTEM image. More intriguingly, the TiO_2 crystallites in the porous structures are crystallographically aligned, giving mesocrystalline characteristics,[31] while the mesopores are well connected (Figure 5b). The propagating direction of individual self-assembling TiO_2 petals is along the *c*-axis (i.e., the [001] direction) of anatase crystal structure.[6] All parallel lattice fringes can be assigned to the interplanar spacing d_{101} (3.5 ± 0.1 Å), while the atomic defects and planar mismatches in or among the crystallites are visualized. The mesocrystalline nature of anatase TiO_2 petals was further confirmed with our heat-treatment experiments (up to 900 °C), through which the internal pores merged and diffused to surface region, and the mesocrystalline TiO_2 petals became essentially single-crystalline (in rutile phase) upon the heating, as illustrated by our TEM/SEM combined microscopic investigation reported in Figure 6. In this agreement, the specific area of TiO_2/CNTs was reduced from 116 m^2/g to 97 m^2/g (heated at 300 °C) and further to 7.5 m^2/g (heated at 900 °C). The concave vacant spaces on the crystal petals are now bounded with low Miller indexed facets, after this topotactic rutilization (Figure 6). In this regard, crystal phase and surface area of the oxide overlayer can also be fine-tuned by additional heat-treatments.

(31) Cölfen, H.; Antonietti, M. *Angew. Chem., Int. Ed.* **2005**, *44*, 2–17.

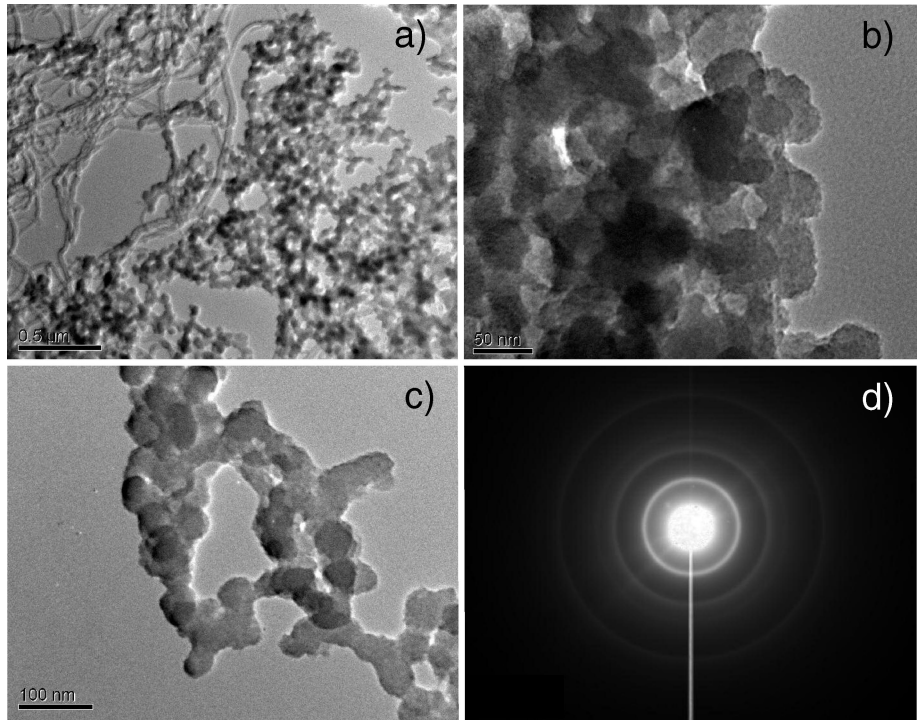

Figure 7. Overall product morphology of pearl-like TiO_2 nanoparticle aggregates together with CNTs (a, TEM image), detailed views on TiO_2 nanoparticle aggregates (b and c, TEM images), and a SAED ring pattern (d) which was measured from the sample displayed in (c). The synthesis was carried out in an open system (see Experimental Section).

In order to have chemical information on surface, the TiO_2/CNTs samples have been further explored with X-ray photoelectron spectroscopy. In Figure 5c, the main C 1s peak at binding energy (BE) of 284.6 eV is assigned to adventitious carbon and sp^2-hybridized carbon of the CNTs (i.e., a small fraction of CNTs is not entirely covered by the TiO_2 coating).[29,30] The broad peak located at 285.2 eV is known to be defect-containing sp^2-hybridized carbons,[29] which are believed to serve as initial nucleation sites for TiO_2 deposition. In Figure 5d, two Ti 2p peaks (Ti $2p_{3/2}$ and Ti $2p_{1/2}$) at 458.6 and 464.3 eV are characteristics of the phase-pure TiO_2,[29,30] noting that the photoelectron signals were generated from the outer surface of TiO_2. Corresponding to this metal oxide, the O 1s peak at 529.9 eV in Figure 5e is associated to the oxygen anions in the lattice, while the broader peak centered at 531.6 eV to Ti-OH and/or C═O, C—O and O—C═O surface species.[29,30]

It should be mentioned that most of reported mesocrystals and mesoporosity were obtained with assistances of organic templates and/or guiding agents such as surfactants and polymeric networks.[31] In contrast, our present approach does not need any of these organic additives, templates and/or guiding agents. The exact formation of mesocrystalline structure without the assistance of organics has not been well understood at this time. One very plausible mechanism is that the mesoporous products are simply resulted from a recrystallization event (i.e., a transformation from amorphous state (less dense phase) to crystalline state (more dense phase), leaving some pace behind.[32] Based on eq 1, on the other hand, one may also recognize that the formation of TiO_2 is accompanied with production of a significant amount of HF gas, because there will be 4 moles of HF produced for every mole of TiF_4 consumed. Under our mild reaction conditions (at 60 °C and slightly over 1 atm; without stirring), part of gaseous HF might be trapped/adsorbed on growing TiO_2 crystallites. This gas–solid interface may prevent the crystallites from further growth, as the supply of TiF_4 from liquid is terminated, noting that new growth can always takes place in any available liquid–solid interfaces, resulting in well connected mesocrystalline structure. It should be mentioned that nanoscopic gas bubbles are not stable due to their high capillary pressures. But their momentary existence on the growth front may be attributable to the initiation of directional nucleation and subsequent growth. Although the above proposed mechanisms can account for our observations, other less plausible mechanisms (such as oriented aggregation of performed nanoparticles or dissolution of solid)[33,34] cannot be entirely ruled out at this stage. We had also carried out a growth experiment without using the parafilm and the plastic cap, i.e., the growth conducted was a semibatch process under normal atmospheric pressure (i.e., an open reaction system; see Experimental Section). Some of the product morphologies of this experiment are displayed in Figure 7. As can be observed, isolated TiO_2 nanoparticulate aggregates were formed together with the TiO_2/CNTs and uncovered CNTs. Because the HF gas bubbles in this case can be depleted from the reaction system once they are produced, the formation reaction of TiO_2 can be expected

(32) Wang, T. X.; Cölfen, H.; Antonietti, M. *J. Am. Chem. Soc.* **2005**, *127*, 3246–3247.
(33) Yang, H. G.; Zeng, H. C. *Angew. Chem., Int. Ed.* **2004**, *43*, 5930–5933.
(34) Liu, B.; Zeng, H. C. *Small* **2005**, *1*, 566–571.

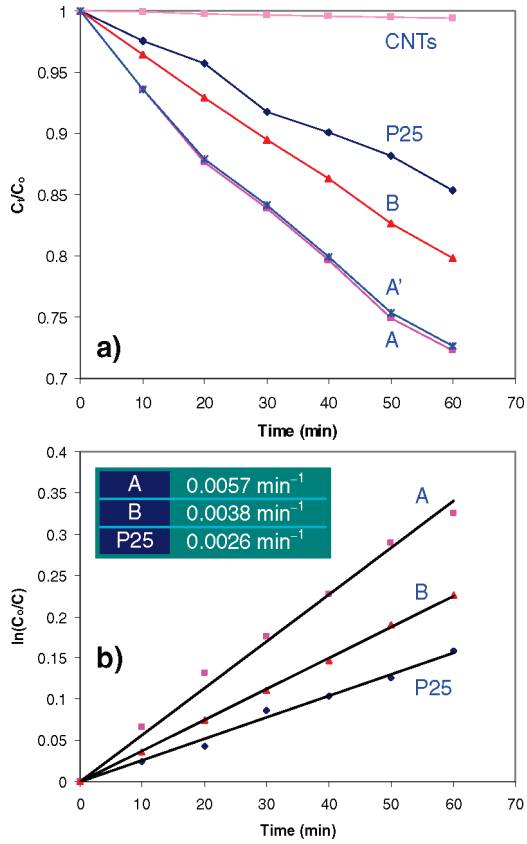

Figure 8. Photocatalysis data: (a) normalized concentration (C/C_0; C_0 and C are initial concentration and concentration at time t of methyl orange) versus reaction time (t) for different samples tested; and (b) kinetic plots based on the data of (a). Apparent rate constants (k_a) are listed in the table of (b). Catalyst preparation (A, Sample A; A′, used Sample A; and B, Sample B) and reaction conditions can be referred to Experimental Section.

to proceed more easily to the right-hand side of eq 1, that is, the growth of TiO_2 does not rely on the CNTs-assisted nucleation that was observed in the preparations of Samples A and B, and a separate phase of TiO_2 is resulted (Figure 7a-c), although this oxide is still in anatase phase (SAED pattern, Figure 7d).

Concerning their actual applications, the mesoporous TiO_2/CNTs were used as solid-state catalysts and further investigated for their photocatalytic activity. In Figure 8, kinetic data of methyl orange degradation using two representative catalysts (Samples A and B) are displayed, together with those of P25 and CNTs for comparison. It is clearly demonstrated that the TiO_2/CNTs catalyst optimized in this work (Sample A) shows the best performance, because its lowering rate in C/C_0 is the fastest among the four samples, where C_0 is the initial concentration of methyl orange and C is the concentration of the reactant at time t. It should be mentioned that the TiO_2 contents in the two catalysts are only about 47.9 wt % and 57.2 wt % of the sample P25. Therefore, the catalytic degradation of organic dye using our catalysts is much more efficient, in comparison to P25 and CNTs. Similar to other studies on organic dyes, the degradation reactions on the catalytic samples can be ascribed to a pseudofirst-order reaction with a simplified Langmuir–Hinshelwood model when C_0 is very small:[35–37]

$$\ln(C_0/C) = k_a t \quad (2)$$

where k_a is the apparent first-order rate constant, as displayed in Figure 8b. The observation on high activity can be attributed to a number of factors: (i) the large specific area of the TiO_2 phase which ensures the highest exposure to the UV light and provides abundant reaction sites for degradation reactions; (ii) through-porosity which allows efficient transports of reactants and products; (iii) the overall oriented attachment among TiO_2 nanocrystallites which minimizes the light reflections and allows the light transmitted to deeper parts (and thus pores) of the TiO_2 petals; and (iv) surface defect sites and conductive CNTs support which may serve as electron reservoirs to suppress the recombination of electron–hole pairs. In addition to the above findings, the role of CNTs on oxygen adsorption and thus on surface hydroxyl radical formation have been recently proposed in a photocatalytic investigation of azo dyes using a series of mixed catalysts of P25 and CNTs.[36] Despite the above identified factors, we still recognize that the very complex nature of the photocatalytic activity remains to be fully explored. Finally, it should be mentioned that the catalyst prepared with the present method is both chemically and structurally stable. The catalysts could maintain their excellent activity (see Sample A′ in Figure 8a), and the TiO_2 petals did not indicate any detachment from their CNTs support after use (see Supporting Information, SI-4).

Conclusions

In summary, we have developed a one-pot solution approach to combine two most studied materials, anatase TiO_2 and CNTs, into binary nanocomposites. With this surfactant-free method, surface coverage, surface area, and crystallite orientation of anatase TiO_2 on the CNTs support can be facilely manipulated. Under mild reaction conditions, in particular, [001]-oriented petal-like TiO_2 mesocrystals have been evenly grown onto CNTs in aqueous solution, with TiO_2 crystallites of 2–4 nm and a very uniform size distribution of mesopores centered at 2.5 nm. Our investigation also indicates that the as-prepared TiO_2/CNTs nanocomposites are highly active and robust for photocatalytic applications, without additional treatments. Because of the simple reaction conditions (at 60 °C and slightly higher than 1 atm), large scale production of the CNTs supported mesocrystals of TiO_2 is also anticipated.

Acknowledgment. The authors gratefully acknowledge the financial support of the Ministry of Education, Singapore. B.L. would like to thank the National University of Singapore for providing his postgraduate scholarship.

Supporting Information Available: EDX, DTG, FESEM, and TEM results (PDF). This material is available free of charge via the Internet at http://pubs.acs.org.

CM800040K

(35) Wang, X. H.; Li, J.-G.; Kamiyama, H.; Moriyoshi, Y.; Ishigaki, T. *J. Phys. Chem. B* **2006**, *110*, 6804–6809.
(36) Yu, Y.; Yu, J. C.; Chan, C.-Y.; Che, Y.-K.; Zhao, J.-C.; Ding, L.; Ge, W.-K.; Wong, P.-K. *Appl. Catal., B* **2005**, *61*, 1–11.
(37) Li, J.; Zeng, H. C. *Chem. Mater.* **2006**, *18*, 4270–4277.